

# Precision reconstruction of rational CFT from exact fixed point tensor network

Gong Cheng,<sup>1,2,\*</sup> Lin Chen,<sup>3,\*</sup> Zheng-Cheng Gu,<sup>4,†</sup> and Ling-Yan Hung<sup>5,‡</sup>

<sup>1</sup>*Department of Physics, Virginia Tech, Blacksburg, VA 24060, USA*

<sup>2</sup>*Maryland Center for Fundamental Physics, University of Maryland, College Park, MD 20740, USA*

<sup>3</sup>*School of Physics and Optoelectronics, South China University of Technology, Guangzhou 510641, China*

<sup>4</sup>*Department of Physics, The Chinese University of Hong Kong, Shatin, New Territories, Hong Kong, China*

<sup>5</sup>*Yau Mathematical Sciences Center, Tsinghua University, Haidian, Beijing 100084, China*

(Dated: November 7, 2024)

The novel concept of entanglement renormalization and its corresponding tensor network renormalization technique have been highly successful in developing a controlled real space renormalization group (RG) scheme. Numerically approximate fixed-point (FP) tensors are widely used to extract the conformal data of the underlying conformal field theory (CFT) describing critical phenomena. In this paper, we present an explicit analytical construction of the FP tensor for 2D rational CFT. We define it as a correlation function between the "boundary-changing operators" on triangles. Our construction fully captures all the real-space RG conditions. We also provide concrete examples, such as Ising, Yang-Lee and Tri-critical Ising models to compute the scaling dimensions explicitly based on the corresponding FP tensor. Interestingly, our construction of FP tensors is closely related to a strange correlator, where the holographic picture naturally emerges. Our results also open a new door towards understanding CFT in higher dimensions.

## INTRODUCTION

In the past two decades, the novel concept of entanglement renormalization [1–5] has been developed to study critical systems. In particular, computationally efficient algorithms has been proposed based on tensor network techniques, such as various schemes of tensor network renormalization (TNR) [2, 5–10]. It is found that even with a moderate size of bond dimensions kept in the coarse graining procedure, there are lots of important information such as central charge, scaling dimensions and operator product expansion (OPE) coefficient of conformal field theory (CFT) can be read off from the fixed point (FP) tensors, which are approximate fixed points of the TNR algorithms [5, 10]. Despite the huge successes in numerically extracting conformal data through tensor network simulations, the analytical construction of FP tensors for critical systems remains a significant challenge. While progress has been made in understanding the components of FP tensors associated with primary fields [11, 12], generalizing these constructions for descendant fields remains unclear. On the other hand, the recently proposed holographic picture and generalized symmetry description [13–15] for CFT suggest that the complete algebraic structure of FP tensors might provide us an alternative way to understand CFT, which will lead to a revolution in modern physics.

In this paper, we demonstrate that the collection of open string correlation functions conformally related to an open pair of pants in every rational CFT (RCFT) yields an exact infinite-dimensional FP tensor. By tiling these correlators over a given manifold and summing over all intermediate states, including primaries and descendants, we obtain the RCFT path integral. However, this tiling process leaves behind holes, which must be recon-

ciled for the correlators to match with an FP tensor. Previous research [16] introduced shrinkable boundary conditions that address this problem and was further studied in [17]. By combining these boundary conditions with the open correlators, we achieve a field theoretical construction of tensors that satisfy the expected properties of a FP tensor. To validate our approach, we provide explicit numerical examples, focusing on the Ising model. Our results demonstrate convincingly that our proposed FP tensors can accurately recover the closed spectrum of the exact CFT when tiling a cylinder.

Finally, we stress that our construction of FP tensors coincides with constructing an eigenstate  $\langle \Omega |$  of the topological RG operator associated to a fusion category  $\mathcal{C}$  [18, 19], and expressing the CFT partition function as a *strange correlator* [20], namely  $Z_{CFT} = \langle \Omega | \Psi \rangle$ , where  $|\Psi\rangle$  is the ground state wave-function of the Levin-Wen model [21], or Turaev-Viro topological quantum field theory (TQFT) [22], associated also to category  $\mathcal{C}$  [23].

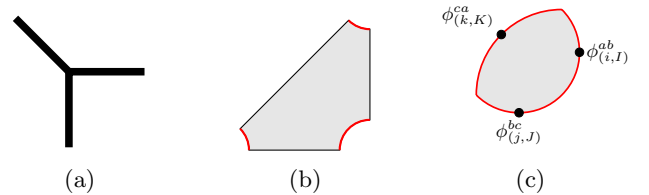


FIG. 1: (a) denotes the rank-3 tensor, corresponds to a path integral over the shaded region (b). (c) denotes correlation function of three local operators on a disk with conformal boundary condition on the red edge.

## THE STRUCTURE OF FP TENSOR

The FP tensor we propose, denoted as  $\mathcal{T}_{(i,I)(j,J)(k,K)}^{abc}$ , comprises nine indices. The labels  $a, b, c$  correspond to the conformal boundary conditions of the RCFT, while  $i, j, k$  represent the labels of the RCFT primaries, and the indices  $I, J, K$  pertain to the descendants of their respective primaries. In the RCFT,  $a, b, c$  and  $i, j, k$  take values from a finite set, while  $I, J, K$  live in an infinite-dimensional space. Consequently, the exact FP tensors possess an infinite bond dimension, as expected. The FP tensor,  $\mathcal{T}_{(i,I)(j,J)(k,K)}^{abc}$ , can be interpreted as the path integral of the CFT within an open triangle. See Fig. 1b. To regulate the path integral, we slightly modify the corners of the triangle and impose conformal boundary conditions labeled as  $a, b$ , and  $c$  at each respective corner. The edges of the triangle correspond to states that can be mapped to boundary-changing operators that connect the two conformal boundaries associated with the given edge (See Fig. 1c).

To show that they correspond to FP tensors, we need to demonstrate three properties: (a) the FP tensors should satisfy crossing relations; (b) FP tensors covering a large patch upon contraction reproduce exactly the same FP tensors covering a smaller patch; (c) Tiling the FP tensors on a surface and assigning appropriate contraction of the indices recover the CFT path-integral on the surface. These conditions (a) and (b) are illustrated in Fig. 4 and Fig. 6. As we will see, these requirements ensure that the FP tensors reconstruct the CFT partition function exactly.

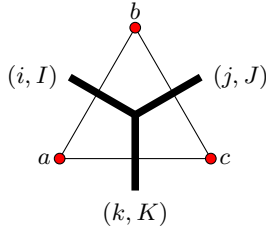


FIG. 2: Diagrammatical representation of the tensor. The base triangle denotes the structure coefficient  $C_{ijk}^{abc}$ , and the rank-3 tensor on top of it denotes the conformal block  $\alpha_{IJK}^{ijk}$  which carries descendants information.

In general, the FP tensor can be decomposed as:

$$\mathcal{T}_{(i,I)(j,J)(k,K)}^{abc} = \alpha_{IJK}^{ijk} C_{ijk}^{abc} \quad (1)$$

This is because a three-point correlation function of three boundary operators carries two parts, represented diagrammatically in Fig. 2, namely the structure coefficients  $C_{ijk}^{abc}$  and the 3-point conformal blocks carrying the dependence of the correlation function on the precise descendant in the primary families, the location of insertions, and the precise shape of the manifold in which op-

erators are inserted. To set our notations, the three point correlation functions of three primary boundary changing operators on the upper-half-plane (UHP) is given by:

$$\langle O_{(i,0)}^{ab}(x_1) O_{(j,0)}^{bc}(x_2) O_{(k,0)}^{ca}(x_3) \rangle_{\text{UHP}} = C_{ijk}^{abc} \beta_{000}^{ijk}(x_1, x_2, x_3), \quad (2)$$

$$\beta_{000}^{ijk}(x_1, x_2, x_3) = \frac{1}{|x_1 - x_2|^{h_i+h_j-h_k} |x_1 - x_3|^{h_i+h_k-h_j} |x_3 - x_2|^{h_k+h_j-h_i}}, \quad (3)$$

where  $I = J = K = 0$  denotes the fact that the inserted operators are all primaries. Conformal blocks involving other descendants where  $I, J, K \neq 0$  can be generated by repeated use of the Virasoro or generally Kac-Moody operators in the primaries.

In our proposed FP tensor,  $\alpha_{IJK}^{ijk}$  is related to  $\beta_{IJK}^{ijk}$  by some conformal maps  $\chi_{1,2,3}$ ,

$$C_{ijk}^{abc} \alpha_{IJK}^{ijk} = \langle \chi_{1*} O_{(i,I)}^{ab}(x_1) \chi_{2*} O_{(j,J)}^{bc}(x_2) \chi_{3*} O_{(k,K)}^{ca}(x_3) \rangle_{\text{UHP}}. \quad (4)$$

where the conformal transformations  $\chi_{1,2,3}$  map the amplitude on triangle to three point function on UHP, see Fig. 3. As we will explain with more detail in the next section, each  $\chi_i$  is a composition of two conformal maps. The first maps the state on each edge in Fig. 1b to local operator in Fig. 1c, and the second maps the three point function on disk in Fig. 1c to UHP, allowing us to calculate it using  $\beta_{IJK}^{ijk}$ . The coordinates  $x_{1,2,3} = \chi_{1,2,3}(0)$  are fixed and suppressed in the following.

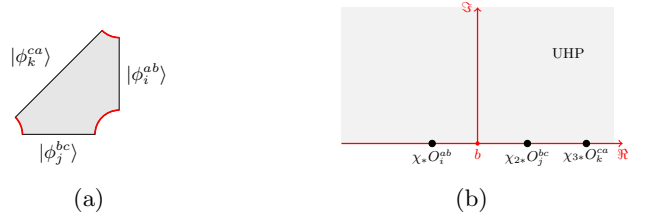


FIG. 3: Conformal transformation that maps the amplitude in triangular region to upper-half-plane with three local operators inserted on the real-axis.

These  $\alpha_{IJK}^{ijk}$ 's are called 3-point conformal blocks and fully determined by conformal symmetry. They satisfy:

$$\sum_M \alpha_{IJM}^{ijm} \alpha_{MKL}^{mkl} = \sum_{n,N} [F_l^{ijk}]_{mn}^{\text{blocks}} \alpha_{INL}^{inl} \alpha_{JKN}^{jkn}, \quad (5)$$

where  $[F_l^{ijk}]_{mn}^{\text{blocks}}$  are the crossing coefficients characterizing this RCFT. The same matrix  $F^{\text{blocks}}$  also relate structure coefficients  $C_{ijk}^{abc}$  through the equation,

$$\sum_m [F_l^{ijk}]_{mn}^{\text{blocks}} C_{ijm}^{abc} C_{mkl}^{acd} = C_{inl}^{abd} C_{jkn}^{bcd}. \quad (6)$$

This guarantees the proposed FP tensor satisfies the crossing relation in condition (a).

$$\begin{aligned} & \sum_{m,M} \mathcal{T}_{(i,I)(j,J)(m,M)}^{abc} \mathcal{T}_{(m,M)(k,K)(l,L)}^{acd} \\ &= \sum_{n,N} \mathcal{T}_{(i,I)(n,N)(l,L)}^{abd} \mathcal{T}_{(j,J)(k,K)(n,N)}^{bcd}. \end{aligned} \quad (7)$$

Diagrammatically, this is illustrated in Fig. 4, which follows from the crossing symmetry of the RCFT (see Fig. 5).

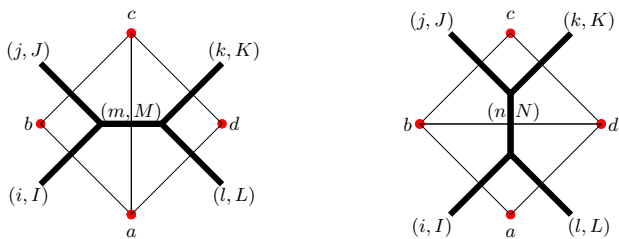


FIG. 4: Crossing relation of FP tensor.

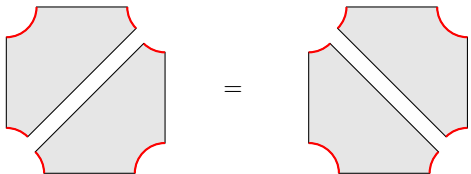


FIG. 5: Crossing symmetry: two ways of gluing CFT path-integral on triangles are equivalent.

The FP tensor also satisfies the coarse graining condition (b), which is illustrated in Fig. 6.

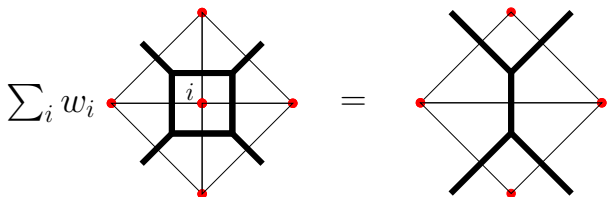


FIG. 6: Coarse graining condition of FP tensor.

We note that the vertex degree of freedom at the center is summed over with a weight  $w_i$ . For a diagonal RCFT,

$$w_i = S_{00}^{1/2} S_{i0}, \quad (8)$$

Physically, the coarse-graining step corresponds to sewing four triangles by contracting the shared descendant labels between neighboring triangles along the shorter edges, as in Fig. 7. However we note that a small hole is left in the middle. In order for the coarse-graining condition to be satisfied, this hole need to disappear.

This can be done by first summing over the conformal boundary conditions with weights given by (8), followed by shrinking the size of hole to zero. The idea of this weighted sum of conformal boundary conditions was initially explored in [16] within the context of entanglement brane boundary conditions. It suggests that the boundaries arising in the computation of the entanglement entropy are artificial and should be "contractible." Another motivation is that the weighted sum makes the boundary transparent to topological defect in CFT [17]. These considerations motivated the use of this particular weighted sum.

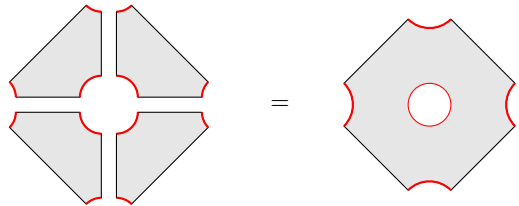


FIG. 7: Gluing four triangles into a square with hole in the center.

The open boundary can be transformed through a modular transformation into a closed conformal boundary Cardy state  $|i\rangle_c$ . It can be shown that the weighted sum of the boundaries yields:

$$\sum_i w_i |i\rangle_c = |0\rangle, \quad (9)$$

where the right-hand side corresponds to the identity of the Ishibashi state. When the size of hole  $r$  is small, the state is evolved by a long Euclidean time and becomes,

$$\begin{aligned} & \lim_{r \rightarrow 0} e^{-H|\log r|} |0\rangle \\ &= e^{\frac{6}{c}\pi|\log r|} \left( |0\rangle + \frac{2}{c} e^{-8\pi|\log r|} L_{-2} \bar{L}_{-2} |0\rangle + \dots \right). \end{aligned} \quad (10)$$

The dominant contribution arises from the leading term, which is the vacuum state. The leading corrections then come from the leading descendant of the vacuum state, which can be viewed as an irrelevant perturbation in the thermodynamic limit of the tiling, as explained in [17]. This boundary conditions are physical reasons behind condition (b) and (c) satisfied by the FP tensor.

The partition function of the CFT on a manifold  $\mathcal{M}$  can be obtained using the following procedure. We begin by triangulating the manifold  $\mathcal{M}$  into a collection of triangles  $\Delta$ . Each edge  $e$  on a triangle is labeled with a pair of primary and descendant labels  $(i, I)$ , and each vertex  $v$  is labeled with a conformal boundary condition  $a$ . On each triangle, we assign a tensor  $\mathcal{T}_{(i,I)(j,J)(k,K)}^{abc}$  based on the labeling of the edges and vertices. The proposed partition function is then given by:

$$Z_M = \sum_{\{(i,I)\}, \{a\}} \prod_v \omega_a \prod_{\Delta} \mathcal{T}_{(i,I)(j,J)(k,K)}^{abc}. \quad (11)$$

## COMPUTING THE CONFORMAL BLOCK

To calculate each component of the FP tensor, we evaluate the conformal block  $\alpha_{IJK}^{ijk}$ , which is calculated by the path-integral on the triangular region. In this article, we provide two methods, one is through the state-operator correspondence. Another method can be found at Supplemental Material. The standard state-operator correspondence allows us to prepare a state  $|O_i^{ab}\rangle$  on the unit semi-circle by inserting local operator  $O_i^{ab}$  at the origin. See the left side of Fig. 8a. Now we find a function  $f(z)$  which maps the semi-disk to a circular segment region, as shown in right side of Fig. 8a. The operator  $O_i^{ab}$  is mapped to  $f_*O_i^{ab}$  inserted on the arc of the segment. Through this map we prepare some state  $|\phi_i^{ab}\rangle$  on the vertical edge of the segment region.

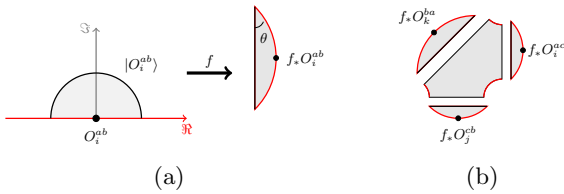


FIG. 8: (a) The semi-disk is mapped to a circular segment region through a function  $f(z)$ . (b) The amplitude of three open states can be calculated by attaching three segment regions along the open boundaries of triangle.

To calculate the amplitude in Fig. 3a we attach these prepared states to the three open boundaries of the triangular region. Diagrammatically, this process is represented by gluing the segments along the three open boundaries as shown in Fig. 8b.

We further require that the prepared states form an orthonormal basis in the Hilbert space of boundary CFT. The inner product of these states is determined by the two-point function on the nut-shaped region as shown in Fig. 9.

$$\langle \phi_i^{ab} | \phi_j^{ba} \rangle = f_*O_j^{ba\dagger} \bullet \bullet f_*O_i^{ab}$$

FIG. 9: The double segment region obtained by gluing two circular segments along the vertical edge.

The condition of orthonormality is expressed through the following equation of two point function on the nut:

$$\langle [f_*O_j^\dagger](-b)[f_*O_i](b) \rangle_{\text{nut}} = \delta_{ij}. \quad (12)$$

where  $b$  is the coordinates of operators on the nut. The two-point function can be readily calculated by observing that the same function  $f(z)$  maps the compactified UHP

to the nut-shaped region. This mapping is a composition of three simple transformations, whose effects are illustrated in Fig. 10,

$$\begin{aligned} f(z) &= \xi \circ \eta \circ \omega(z) \\ \omega(z) &= \frac{1+z}{1-z}, \quad \eta(\omega) = e^{-i\theta} \omega^{\frac{2\theta}{\pi}}, \quad \xi(\eta) = i \frac{\eta-1}{\eta+1}. \end{aligned} \quad (13)$$

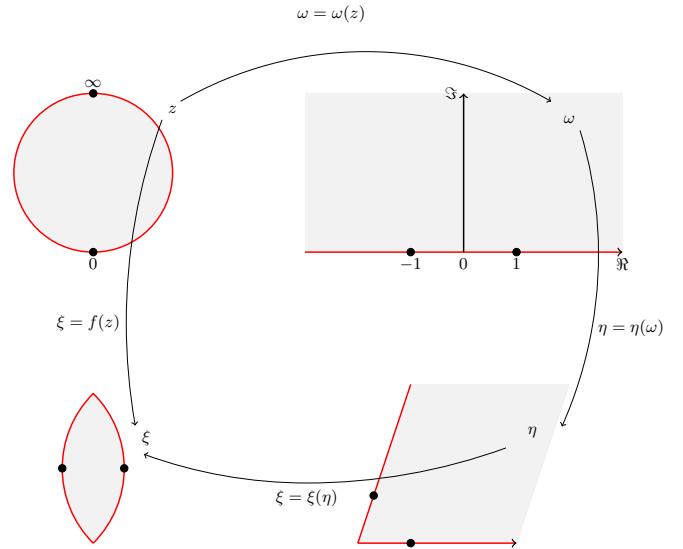


FIG. 10: Conformal map from compactified UHP (top left) to the nut region (bottom left) as composition of three simple maps. Black dots represent location of the operators insertion.

Since  $f(z)$  maps UHP to the nut, the two point function of operator  $f_*O_i^{ab}$  on the nut is equal to the two point function of operator  $O_i^{ab}$  on the UHP.

$$\langle [f_*O_j^{ba\dagger}](-b)[f_*O_i^{ab}](b) \rangle_{\text{nut}} = \langle O_j^{ba\dagger}(\infty)O_i^{ab}(0) \rangle_{\text{UHP}}. \quad (14)$$

Therefore the condition in Eq. (14) is equivalent to finding orthonormal set of basis operators  $O_i^{ab}$ .

Here we have a free parameter  $\theta$  which is the angle of the corner in the segment region (see Fig. 8a). This angle serves as a gauge freedom of our tensor construction. For computation simplicity we choose to set  $\theta = \frac{\pi}{4}$ .

Following the state to operator map, we proceed by shrinking the corners of the triangular region to zero length. This leads to the disk with smooth boundary except for the two cusps. Three operators are inserted on the boundary as shown in Fig. 11a.

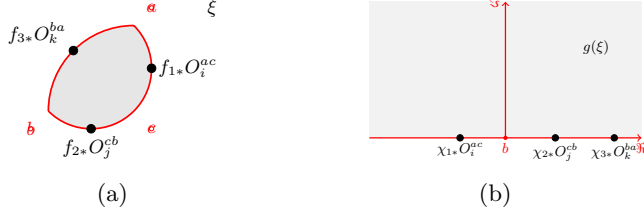


FIG. 11: Conformal transformation  $g(\xi)$  maps the disk with two cusps (a) to the upper-half-plane (b).

Note that the operators inserted at the three different directions are mapped by three functions  $f_1$ ,  $f_2$  and  $f_3$  that are related to  $f$  by translation and rotation according to the orientation of the state in Fig. 8b.

$$\begin{aligned} f_1(z) &= f(z) + 1, & f_2(z) &= -if(z) - i \\ f_3(z) &= \sqrt{2}e^{i\frac{3\pi}{4}}f(z) \end{aligned} \quad (15)$$

They map the origin of Fig. 8a to the three points on the disk in Fig. 11a.

In the final step we find a function  $g(\xi)$  that maps the disk (Fig. 11a) to the UHP (Fig. 11b). Given the gauge choice  $\theta = \frac{\pi}{4}$ , the disk boundary has only two cusps. We choose the function  $g(\xi)$  which maps them to 0 and  $\infty$ . This function be written down explicitly as,

$$g(\xi) = \left(-i\frac{\xi + (1+i)}{\xi - (1+i)}\right)^{\frac{4}{3}}. \quad (16)$$

After applying the conformal transformation  $g(\xi)$ , the operators on the UHP in Fig. 11b becomes  $\chi_{1*}O_1^{ac}(x_1)$ ,  $\chi_{2*}O_2^{cb}(x_2)$  and  $\chi_{3*}O_3^{ba}(x_3)$ , where the  $\chi$ -functions are defined as the following composition of the mapping  $f$  and  $g$ ,

$$\begin{aligned} \chi_1(z) &= g(f(z) + 1), & \chi_2(z) &= g(-if(z) - i), \\ \chi_3(z) &= g(\sqrt{2}e^{i\frac{3\pi}{4}}f(z)). \end{aligned} \quad (17)$$

They map the origin of Fig. 8a to three points on the real axis in Fig. 11b, with coordinates  $x_1 = \chi_1(0)$ ,  $x_2 = \chi_2(0)$ ,  $x_3 = \chi_3(0)$ . So the tensor components are equal to the following three point functions on upper-half-plane,

$$\mathcal{T}_{(I,i)(J,j)(K,k)}^{abc} = \langle \chi_{1*}O_{(I,i)}^{ac}(x_1)\chi_{2*}O_{(J,j)}^{cb}(x_2)\chi_{3*}O_{(K,k)}^{ba}(x_3) \rangle_{UHP}, \quad (18)$$

As a simple example, consider the three boundary operators all being primary fields with conformal dimension  $h_1$ ,  $h_2$  and  $h_3$ . The dependence on conformal boundary condition  $a,b,c$  are only contained in the structure constant  $C_{ijk}^{abc}$ . We write down the conformal block  $\alpha_{IJK}^{ijk}$

as,

$$\begin{aligned} \alpha_{000}^{h_1 h_2 h_3} &= \frac{|\chi_1'(0)|^{h_1} |\chi_2'(0)|^{h_2} |\chi_3'(0)|^{h_3}}{|x_1 - x_2|^{h_1+h_2-h_3} |x_2 - x_3|^{h_2+h_3-h_1} |x_1 - x_3|^{h_1+h_3-h_2}} \\ &\approx 0.265^{h_1+h_2} 0.704^{h_3} \\ &= 0.515^{\Delta_1+\Delta_2} 0.839^{\Delta_3}, \end{aligned} \quad (19)$$

where  $\Delta_i = 2h_i$  are the corresponding bulk conformal dimensions.

## EXAMPLES

### The Ising CFT

In the Ising example, we can put in explicit expressions to the above construction. The closed Ising CFT has three primaries  $\mathcal{C}_{Is} = \{I, \psi, \sigma\}$ . The theory has three conformal boundary conditions. They are labeled as  $\{+, -, f\}$ , corresponding to the respective primaries. The Hilbert space for an interval with left and right boundary given by  $a$  and  $b$  respectively, where  $a, b \in \mathcal{C}_{Is}$  is given by  $\mathcal{H}_{ab} = \oplus_c N_{ab}^c V_c$ , where  $V_c$  is the space corresponding to the primary representation labeled  $a \in \mathcal{C}_{Is}$ , and  $N_{ab}^c \in \mathbb{Z}_{\geq 0}$  are the fusion coefficient among the objects  $\mathcal{C}_{Is}$ , with:  $N_{Ib}^c = \delta_{bc}$ ,  $N_{\sigma\sigma}^c = 1 - \delta_{c\sigma}$ ,  $N_{\sigma a \neq \sigma}^b = \delta_{b\sigma}$ ,  $N_{\psi\psi}^b = \delta_{bI}$ .

The matrix  $[F_l^{ijk}]^{\text{blocks}}$  is provided in Supplemental Material. Using Eq. (33), we calculate the structure coefficients  $C_{ijk}^{abc}$ . Below we list those values other than 1:

$$\begin{aligned} C_{III}^{\pm\pm\pm} &= C_{\psi\psi I}^{\pm\mp\pm} = C_{\sigma\sigma I}^{\pm f\pm} = 2^{\frac{1}{4}}, \\ C_{\sigma\sigma\psi}^{\pm f\mp} &= \frac{1}{2^{\frac{1}{4}}}, C_{\sigma\sigma\psi}^{f+f} = \frac{1}{\sqrt{2}}, C_{\sigma\sigma\psi}^{f-f} = -\frac{1}{\sqrt{2}} \end{aligned} \quad (20)$$

We have to compute the three point functions involving descendants, and then transform them into the needed geometry using the conformal map constructed in the last section. Explicitly, one has to first look for the orthogonal basis of the descendants. For example, in level one, the normalized first descendant  $O^{(-1)}$  is defined as  $\frac{1}{\sqrt{2h}}L_{-1}O$ . It's transformation under the conformal map  $\chi(z)$  is:

$$\chi_*[O^{(-1)}] = |\chi'(0)|^h \left( \chi'(0)O^{(-1)} + \sqrt{\frac{h}{2}} \frac{\chi''(0)}{\chi'(0)} O \right). \quad (21)$$

In the second level, we find three normalized operators,

$$\mathbb{1}^{(-2)} = 2L_{-2}\mathbb{1}, \quad (22)$$

$$\psi^{(-2)} = \frac{6}{25}L_{-2}\psi + \frac{9}{25}L_{-1}^2\psi, \quad (23)$$

$$\sigma^{(-2)} = \frac{16\sqrt{2}}{25}L_{-2}\sigma + \frac{12\sqrt{2}}{25}L_{-1}^2\sigma. \quad (24)$$

and the corresponding transformation rules given by:

$$\chi_*[L_{-2}O] = (\chi')^2 L_{-2}O + \frac{3}{2}\chi'' L_{-1}O + \left( \frac{c\chi'''}{12\chi'} - \frac{c(\chi'')^2}{8(\chi')^2} + \frac{2\chi'''h}{3\chi'} - \frac{(\chi'')^2 h}{4(\chi')^2} \right) O, \quad (25)$$

$$\chi_*[L_{-1}^2O] = (\chi')^2 L_{-1}^2O + (2h+1)\chi'' L_{-1}O + \left( \frac{\chi'''h}{\chi'} + \frac{(\chi'')^2 h(h-1)}{(\chi')^2} \right) O. \quad (26)$$

For higher level descendants, we derive recursive equations to solve all the transformation rules. Additionally, the three-point correlation functions for descendant fields are also calculable by recursive methods. The details are also illustrated in the Supplemental Material. With all the ingredients we numerically calculate the tensors and check the crossing relations (a) and coarse-graining condition (b), keeping only finite number of descendants in each conformal family, up to conformal dimension  $h_{max} = 5$ .

For the crossing symmetry condition (see Fig. 4), we provide an example where we fix the four external legs as  $(\sigma, \sigma, \sigma, \sigma)$  and the four boundary conditions as  $(f, -, f, +)$ . The following contractions are computed,

$$T_{L.H.S.} := T_{\sigma\sigma\mathbb{1}}^{f-f} T_{\sigma\sigma\mathbb{1}}^{f+f} + T_{\sigma\sigma\psi}^{f-f} T_{\sigma\sigma\psi}^{f+f} \quad (27)$$

$$T_{R.H.S.} := T_{\sigma\sigma\psi}^{+f-} T_{\sigma\sigma\psi}^{-f+},$$

where we didn't write the descendant field indices and they are understood as being contracted implicitly. For example,

$$\left( T_{\sigma\sigma\mathbb{1}}^{f-f} T_{\sigma\sigma\mathbb{1}}^{f+f} \right)_{IJKL} := \sum_M T_{(\sigma,I)(\sigma,J)(\mathbb{1},M)}^{f-f} T_{(\sigma,K)(\sigma,L)(\mathbb{1},M)}^{f+f}. \quad (28)$$

In Table I, we list some tensor components of  $T_{L.H.S.}$  vs.  $T_{R.H.S.}$ .

For the coarse-graining condition (see Fig. 6), consider the example of fixing the four external legs as  $(\mathbb{1}, \mathbb{1}, \mathbb{1}, \mathbb{1})$  and the four boundary conditions to be  $(+, +, +, +)$ , we compute the following contraction of four tensors as the the left-hand-side of the equation in Fig. 6:

$$T_{L.H.S.} := [(T_{\mathbb{1}\mathbb{1}\mathbb{1}}^{++++})^4 + (T_{\psi\psi\mathbb{1}}^{+-+})^4 + \sqrt{2}(T_{\sigma\sigma\mathbb{1}}^{+f+})^4]/2\sqrt{2}. \quad (29)$$

Again we didn't write the descendant field indices and they are understood as being contracted implicitly according to Fig. 6. Similarly the right-hand-side of this equation is obtained by contracting two tensors,

$$T_{R.H.S.} = (T_{\mathbb{1}\mathbb{1}\mathbb{1}}^{++++})^2 = \sum_M T_{(\mathbb{1},I)(\mathbb{1},J)(\mathbb{1},M)}^{++++} T_{(\mathbb{1},K)(\mathbb{1},L)(\mathbb{1},M)}^{++++}. \quad (30)$$

In the Table II we present the numerical value of some tensor components. Despite the very small bond dimension, we find that they are satisfied to an accuracy of  $2 \times 10^{-3}$ .

Components	$T_{L.H.S.}$	$T_{R.H.S.}$
0000	0.299	0.307
0010	-0.099	-0.107
0020	0.050	0.063
0030	0.043	0.050
1000	-0.099	-0.107
1010	0.005	0.006
1020	-0.012	-0.014
1030	-0.002	-0.003
2000	0.050	0.063
2010	-0.012	-0.014
2020	0.008	0.012
2030	0.005	0.007
3000	0.043	0.050
3010	-0.002	-0.003
3020	0.005	0.007
3030	0.001	0.001

TABLE I: Table of tensor components for numerically checking the crossing relation.

Components	$T_{R.H.S.}$	$T_{L.H.S.}$
0000	1.015	1.013
0100	0.122	0.124
0200	0.000	-0.000
0300	0.082	0.083
1000	0.122	0.124
1100	0.020	0.021
1200	0.002	0.002
1300	0.014	0.015
2000	0.000	-0.000
2100	-0.002	-0.002
2200	-0.001	-0.001
2300	-0.002	-0.002
3000	0.082	0.083
3100	0.014	0.015
3200	0.002	0.002
3300	0.010	0.010

TABLE II: Table of tensor components for numerically checking the coarse-graining condition.

Finally, We demonstrate that our proposed FP tensor constructed from open correlation functions can indeed recover the closed spectrum with surprisingly high accuracy despite keeping only very few descendants in each family. The cylinder is constructed using 4 squares formed out of 8 triangles, as shown in Fig. 12. The labels of the conformal boundaries at the left and the right edge of the cylinders are treated alongside the primaries and descendent labels of the FP tensors as input and output indices of the cylinder. In our notation, the transfer matrix is denoted by  $M_{aiI,bjJ}$ . The indices  $aiI$  is collective representation of all the confor-

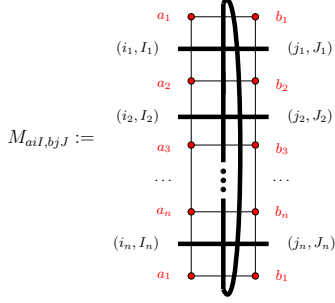


FIG. 12: The transfer matrix

States	Numerical dim	Accurate dim
$\mathbb{1}$	0.0000	0.0000
$\sigma$	0.1250	0.1250
$\psi$	0.9989	1.0000
$\partial\sigma, \bar{\partial}\sigma$	1.1253	1.1250
$\partial\psi, \bar{\partial}\psi$	2.0004	2.0000
$\mathbb{1}^{(-2)}, \bar{\mathbb{1}}^{(-2)}$	1.9986	2.0000
$\partial\bar{\partial}\sigma$	2.1099	2.1250
$\sigma^{(-2)}, \bar{\sigma}^{(-2)}$	2.1208	2.1250
$\partial\bar{\partial}\psi$	2.9517	3.0000
$\partial^2\psi, \bar{\partial}^2\psi$	3.0030	3.0000
$\mathbb{1}^{(-3)}, \bar{\mathbb{1}}^{(-3)}$	2.9496	3.0000
$\bar{\partial}\sigma^{(-2)}, \partial\bar{\sigma}^{(-2)}$	2.9900	3.1250
$\partial\sigma^{(-2)}, \bar{\partial}\bar{\sigma}^{(-2)}$	3.1167	3.1250
$\sigma^{(-3)}, \bar{\sigma}^{(-3)}$	3.1291	3.1250
$\mathbb{1}^{(-2, -2)}$	4.0323	4.0000

TABLE III: Ising model: conformal dimensions from fixed-point tensor vs. exact value. Cylinder length  $L=4$ , descendant level cut=5.

mal boundary labels, primary labels and descendant labels. That is  $a = \{a_1, a_2, \dots, a_n\}$ ,  $i = \{i_1, i_2, \dots, i_n\}$  and  $I = \{I_1, I_2, \dots, I_n\}$ . One can solve for the spectrum of the cylinder, which is listed in the Table III. In the Supplemental Material we provide details on how the numerical conformal dimension converges towards the precise value as we increase the cutoff in descendant level.

The central charge can also be obtained, as explained in Supplemental Material. Here we list the central charge value vs. the descendant level cut-off in Table IV.

descendant	0	1	2	3	4	exact
$c_{\text{Ising}}$	0.4565	0.4900	0.5048	0.5033	0.4975	0.5

TABLE IV: Ising model: central charge computed from FP tensor as function of the descendant level cut-off.

States	Numerical dim	Accurate dim
$\tau$	-0.403	-0.400
$\mathbb{1}$	0.000	0.000
$\partial\tau, \bar{\partial}\tau$	0.598	0.600
$\tau^{(2)}, \bar{\tau}^{(2)}$	1.591	1.600
$\partial\bar{\partial}\tau$	1.600	1.600
$\mathbb{1}^{(2)}, \bar{\mathbb{1}}^{(2)}$	1.996	2.000
$\bar{\partial}\tau^{(2)}, \partial\bar{\tau}^{(2)}$	2.530	2.600
$\tau^{(3)}, \bar{\tau}^{(3)}$	2.594	2.600
$\mathbb{1}^{(3)}, \bar{\mathbb{1}}^{(3)}$	2.939	3.000

TABLE V: Yang-Lee model: conformal dimension from fixed point tensor vs. exact value. Cylinder length  $L=6$ , descendant cut at level 3.

### More examples - The Yang-Lee CFT and tri-critical Ising CFT

In this section, we present numerical results for Yang-Lee CFT and tri-critical Ising CFT. Note that Yang-Lee is a non-unitary CFT, with negative state norm and negative conformal dimension. This renders the some of the tensor componets to take complex value. Despite this we still able to recover the bulk state conformal spectrum by diagonalizing the transfer matrix.

Yang-Lee model has two primary operators, denoted by  $\mathbb{1}$  and  $\tau$ , with conformal dimension 0 and  $-\frac{2}{5}$ . The fusion rule is  $\tau \times \tau = \mathbb{1} + \tau$ . We also label the corresponding conformal boundary condition by  $\{\mathbb{1}, \tau\}$ . The structure constants are given below,

$$\begin{aligned}
C_{III}^{III} &= 1, C_{III}^{\tau\tau\tau} = -1.272i, C_{\tau\tau\tau}^{\tau\tau\tau} = -1.272i \\
C_{\tau\tau\tau}^{\tau I\tau} &= -1.272i, C_{\tau\tau\tau}^{I\tau I} = 1, C_{\tau\tau\tau}^{\tau I\tau} = -1.560, \\
C_{\tau\tau\tau}^{\tau\tau\tau} &= -2.523.
\end{aligned} \tag{31}$$

In Table V we list the bulk conformal dimension obtained from the FP tensor and compare them with the exact values.

For tri-critical ising CFT, the primary fields are labeled by  $\mathbb{1}, \Phi, \Psi, \Xi, \Lambda$  and  $\Omega$ , with corresponding conformal dimension  $\{0, \frac{1}{10}, \frac{3}{5}, \frac{3}{2}, \frac{7}{16}, \frac{3}{80}\}$ . The structure constants can be calculated using Eq. (32) and Eq. (33) and listed in Table XII. We calculate the eigenvalues of the transfer matrix, listed in Table VI, and compare them with the bulk conformal dimension.

Finally we list the value of central charge computed from the transfer matrix in Table VII for both of the two models.

States	Numerical dim	Accurate dim
$\mathbb{1}$	0.0000	0.000
$\Omega$	0.075	0.075
$\Phi$	0.200	0.200
$\Lambda$	0.873	0.875
$\partial\Omega, \bar{\partial}\Omega$	1.076	1.075
$\Psi$	1.196	1.200
$\partial\Phi, \bar{\partial}\Phi$	1.201	1.200
$\partial\Lambda, \bar{\partial}\Lambda$	1.871	1.875
$\mathbb{1}^{(2)}, \bar{\mathbb{1}}^{(2)}$	2.013	2.000
$\partial\bar{\partial}\Omega$	2.064	2.075
$\Omega^{(2)}, \bar{\Omega}^{(2)}$	2.084	2.075
$\Omega^{(2)'}, \bar{\Omega}^{(2)'}$	2.087	2.075
$\partial\bar{\partial}\Phi$	2.190	2.200
$\Phi^{(2)}, \bar{\Phi}^{(2)}$	2.192	2.200
$\partial\Psi, \bar{\partial}\Psi$	2.210	2.200
$\partial\bar{\partial}\Lambda$	2.877	2.875
$\Lambda^{(2)}, \bar{\Lambda}^{(2)}$	2.878	2.875
$I^{(3)}, \bar{I}^{(3)}$	2.978	3.000
$\Xi$	3.004	3.000

TABLE VI: Tri-critical Ising model: conformal dim from fixed point tensor vs. exact value. Cylinder length  $L=3$ , descendant cut at level 2.

descendant	0	1	2	3	4	exact
$c_{\text{TCIS}}$	0.4024	0.6540	0.6820	0.6964	0.6996	0.7
$c_{\text{YL}}$	-4.7307	-4.4143	4.4029	-4.3997	-4.3998	-4.4

TABLE VII: Central charge computed from FP tensor for Yang-Lee (YL) model and tri-critical Ising (TCIS) model

### FP TENSORS AS EIGENSTATES OF TOPOLOGICAL RG OPERATORS

While the FP tensor can be understood directly as a CFT correlation function without explicit reference to an associated 3d TQFT, it is an important observation that these FP tensors follows from an exact eigenstate of the topological RG operator [18, 24], and the CFT partition function can be written explicitly as a *strange correlator*.

To appreciate this connection, recall that the label set of primaries in an RCFT are objects in a modular fusion category  $\mathcal{C}$ . Here we focus on diagonal RCFT so that the conformal boundary conditions are also labeled by objects in  $\mathcal{C}$ . It is convenient to re-scale the three point conformal block  $\alpha_{IJK}^{ijk} = \mathcal{N}_{ijk} \gamma_{IJK}^{ijk}$ , where [25],

$$\mathcal{N}_{ijk} = \sqrt{\theta(i, j, k) / \sqrt{d_i d_j d_k}}, \quad (32)$$

where  $\theta(i, j, k) = d_i / [F^{jkk}]_{1i}^{\text{blocks}}$ , and  $d_i$  is the quantum dimension of object  $i$ , which is related to the modular

matrix by  $d_i = S_{0i}/S_{00}$  for a diagonal RCFT. The value of the FP tensor (1) does not change, except that it is decomposed instead as  $\mathcal{T}_{(i,I)(j,J)(k,K)}^{abc} = \gamma_{IJK}^{ijk} \hat{C}_{ijk}^{abc}$ . On this basis, the structure coefficients  $\hat{C}_{ijk}^{abc}$  of a diagonal RCFT (including the Ising CFT described above) can be written simply as [26],

$$\hat{C}_{ijk}^{abc} = (d_i d_j d_k)^{1/4} \left[ \begin{array}{ccc} i & j & k \\ c & a & b \end{array} \right], \quad (33)$$

where the square bracket denotes the quantum 6j-symbols of the modular tensor category  $\mathcal{C}$  associated to the RCFT in with tetrahedral symmetry and chosen normalization. Several components in this gauge involving the identity label are fixed to the values reviewed in the Supplemental Material. All two point correlations are also normalised. These  $\gamma_{IJK}^{ijk}$  inherit the crossing relation of (5), with the crossing kernel re-scaled as:

$$[F_l^{ijk}]_{mn} = [F_l^{ijk}]_{mn}^{\text{blocks}} \frac{\mathcal{N}_{jkn} \mathcal{N}_{inl}}{\mathcal{N}_{ijm} \mathcal{N}_{mkl}}. \quad (34)$$

These re-scaled crossing kernels  $[F_l^{ijk}]_{mn}$  is related to the quantum 6j-symbol above by:

$$[F_l^{ijk}]_{mn} = \sqrt{d_m d_n} \left[ \begin{array}{ccc} i & j & m \\ k & l & n \end{array} \right]. \quad (35)$$

The explicit values of  $[F_l^{ijk}]_{mn}$  and  $[F_l^{ijk}]_{mn}^{\text{block}}$  for the Ising CFT are given in the Supplemental Material. Now it should be obvious that (11) can be rewritten as a strange correlator  $Z_M = \langle \Omega | \Psi \rangle$ , where  $|\Psi\rangle$  is the ground state of the Levin-Wen model corresponding to the fusion category  $\mathcal{C}$ . It is well known that such a wave-function on a two dimension surface can be constructed using the Turaev Viro formulation of TQFT path-integral over a triangulated three ball [22]. For a surface triangulation that matches the tiling as specified in (11), the Levin-Wen ground state wavefunction can be written as [22, 27, 28]:

$$|\Psi\rangle = \sum_{\{a_v\}} \sum_{\{i\}} \prod_e d_i^{1/2} \prod_v \omega_a \prod_{\Delta} \left[ \begin{array}{ccc} i & j & k \\ c & a & b \end{array} \right] |\{i\}\rangle, \quad (36)$$

The ket  $|\{i\}\rangle$  are basis states living on the edges which carries a label  $i \in \mathcal{C}$ , and

$$\langle \Omega | = \sum_{\{(i,I)\}} \langle \{i\} | \prod_{\Delta} \gamma_{IJK}^{ijk}. \quad (37)$$

The crossing relation (5), together with (9) guarantees that  $\langle \Omega |$  is an eigenstate of the RG operator proposed in [24]. We note that the entanglement brane boundary condition (9) follows simply from the prescription of the Turaev-Viro formation of the path-integral. The weights assigned to each internal edge that is summed agrees with the weighted sum of the Cardy states in (9). In



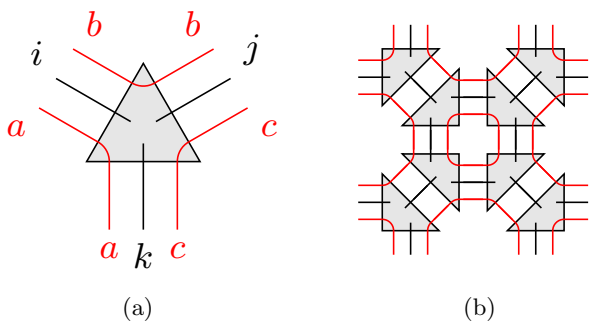


FIG. 13: (a) Triple-line tensor that describes the Levin-Wen ground state. (b) Tiling the tensors into a tensor network to represent the wavefunction  $|\Psi\rangle$ .

other words, the associated 3d TQFT constructed from  $\mathcal{C}$  knows about how to close holes in the RCFT.

When constructing non-diagonal RCFTs, the boundary conditions of the CFT correspond to corner variables placed on triangles, which are generally labeled by objects from a "module category"  $\mathcal{M}_{\mathcal{C}}$  associated with the fusion category  $\mathcal{C}$ . According to the TQFT framework [22], the corner variable should be summed with the weights given by the quantum dimension of the label as an object in the module category. This summation procedure yields the appropriate entanglement brane boundary conditions for general RCFTs. The strange correlator representation of the exact two-dimensional CFT partition function serves as an explicit, practical, and easily computable realization of the holographic relationship between a quantum field theory with categorical symmetry and a TQFT in one higher dimension, as advocated in Ref. [29, 30].

## CONCLUSION AND DISCUSSION

In conclusion, we present a concrete construction of FP tensors for RCFTs based on the holographic principle. Specifically, the FP tensor can be viewed as a correlation function of RCFT involving "boundary-changing operators" defined on triangles. Our proposed construction of the FP tensor naturally fulfills all the requirements of real space RG conditions. This approach provides a novel avenue for exploring the FP tensor of conformal field theory in higher dimensions, offering exciting possibilities for further investigation.

Despite satisfying all the real-space RG conditions, constructing the conformal map  $\chi$  for the FP tensor still poses a challenge due to gauge freedom. We address this issue in the Supplemental Material, where we discuss two distinct conformal maps derived using different methodologies. One of these constructions involves a continuous parameter  $\theta$ , which, when adjusted, has the potential to generate a continuous spectrum of valid FP tensors.

While the gauge freedom complicates direct comparisons between our constructed tensor components and those obtained numerically, the successful reproduction of the bulk states spectrum, while satisfying all RG conditions, serves as a robust validation of our approach. Finally, we stress that our constructions can be naturally generalized into higher dimensions, which might allow us to reformulate all CFTs in terms of tensor networks.

## ACKNOWLEDGMENTS

We acknowledge useful discussions with Xiaogang Wen, Shuheng Shao, Yikun Jiang, Bingxin Lao, Nicolai Reshetikhin, Gabriel Wong and Xiangdong Zeng. This work is supported by funding from Hong Kong's Research Grants Council (GRF no.14301219, no.14303722) and Direct Grant no. 4053578 from The Chinese University of Hong Kong. LYH acknowledges the support of NSFC (Grant No. 11922502, 11875111). LC acknowledges the support of NSFC (Grant No. 12305080) and the start up funding of South China University of Technology. GC acknowledges the support from Commonwealth Cyber Initiative at Virginia Tech, U.S. Department of Energy, Office of Science, Office of Advanced Scientific Computing Research.

---

\* These authors contribute equally.

† corresponding to: zcgu@phy.cuhk.edu.hk

‡ corresponding to: lyhung@tsinghua.edu.cn

- [1] G. Vidal, Entanglement renormalization, *Phys. Rev. Lett.* **99**, 220405 (2007).
- [2] Z.-C. Gu, M. Levin, and X.-G. Wen, Tensor-entanglement renormalization group approach as a unified method for symmetry breaking and topological phase transitions, *Phys. Rev. B* **78**, 205116 (2008).
- [3] G. Evenbly and G. Vidal, Algorithms for entanglement renormalization, *Phys. Rev. B* **79**, 144108 (2009).
- [4] R. N. C. Pfeifer, G. Evenbly, and G. Vidal, Entanglement renormalization, scale invariance, and quantum criticality, *Phys. Rev. A* **79**, 040301 (2009).
- [5] Z.-C. Gu and X.-G. Wen, Tensor-entanglement-filtering renormalization approach and symmetry-protected topological order, *Phys. Rev. B* **80**, 155131 (2009).
- [6] M. Levin and C. Nave, Tensor renormalization group approach to two-dimensional classical lattice models, *Phys. rev. lett.* **99**, 120601 (2007).
- [7] Z.-Y. Xie, H.-C. Jiang, Q.-J. N. Chen, Z.-Y. Weng, and T. Xiang, Second renormalization of tensor-network states, *Phys. rev. lett.* **103**, 160601 (2009).
- [8] Z. Y. Xie, J. Chen, M. P. Qin, J. W. Zhu, L. P. Yang, and T. Xiang, Coarse-graining renormalization by higher-order singular value decomposition, *Phys. Rev. B* **86**, 045139 (2012).
- [9] G. Evenbly and G. Vidal, Tensor network renormalization, *Phys. rev. lett.* **115**, 180405 (2015).

- [10] S. Yang, Z.-C. Gu, and X.-G. Wen, Loop optimization for tensor network renormalization, *Phys. rev. lett.* **118**, 110504 (2017).
- [11] G. Li, K. H. Pai, and Z.-C. Gu, Tensor-network renormalization approach to the  $q$ -state clock model, *Phys. Rev. Res.* **4**, 023159 (2022).
- [12] A. Ueda and M. Yamazaki, Fixed-point tensor is a four-point function, (2023), [arXiv:2307.02523 \[cond-mat.stat-mech\]](#).
- [13] W. Ji and X.-G. Wen, Categorical symmetry and noninvertible anomaly in symmetry-breaking and topological phase transitions, *Phys. Rev. Res.* **2**, 033417 (2020).
- [14] L. Kong, T. Lan, X.-G. Wen, Z.-H. Zhang, and H. Zheng, Algebraic higher symmetry and categorical symmetry: A holographic and entanglement view of symmetry, *Phys. Rev. Res.* **2**, 043086 (2020).
- [15] A. Chatterjee and X.-G. Wen, Holographic theory for continuous phase transitions: Emergence and symmetry protection of gaplessness, *Phys. Rev. B* **108**, 075105 (2023).
- [16] L. Y. Hung and G. Wong, Entanglement branes and factorization in conformal field theory, *Phys. Rev. D* **104**, 026012 (2021), [arXiv:1912.11201 \[hep-th\]](#).
- [17] E. M. Brehm and I. Runkel, Lattice models from CFT on surfaces with holes: I. Torus partition function via two lattice cells, *J. Phys. A* **55**, 235001 (2022), [arXiv:2112.01563 \[cond-mat.stat-mech\]](#).
- [18] R. Vanhove, M. Bal, D. J. Williamson, N. Bultinck, J. Haegeman, and F. Verstraete, Mapping topological to conformal field theories through strange correlators, *Phys. Rev. Lett.* **121**, 177203 (2018).
- [19] D. Aasen, P. Fendley, and R. S. K. Mong, Topological Defects on the Lattice: Dualities and Degeneracies, (2020), [arXiv:2008.08598 \[cond-mat.stat-mech\]](#).
- [20] Y.-Z. You, Z. Bi, A. Rasmussen, K. Slagle, and C. Xu, Wave Function and Strange Correlator of Short Range Entangled states, *Phys. Rev. Lett.* **112**, 247202 (2014), [arXiv:1312.0626 \[cond-mat.str-el\]](#).
- [21] M. A. Levin and X.-G. Wen, String net condensation: A Physical mechanism for topological phases, *Phys. Rev. B* **71**, 045110 (2005), [arXiv:cond-mat/0404617](#).
- [22] V. G. Turaev and O. Y. Viro, State sum invariants of 3 manifolds and quantum 6j symbols, *Topology* **31**, 865 (1992).
- [23] For a physics review of Turaev-Viro models one can consult for example [19].
- [24] L. Chen, H. Zhang, H.-C. Zhang, K.-X. Ji, C. Shen, R.-s. Wang, X.-d. Zeng, and L.-Y. Hung, Exact Holographic Tensor Networks – Constructing  $CFT_D$  from  $TQFT_{D+1}$ , (2022), [arXiv:2210.12127 \[hep-th\]](#).
- [25] T. Kojita, C. Maccaferri, T. Masuda, and M. Schnabl, Topological defects in open string field theory, *JHEP* **04**, 057, [arXiv:1612.01997 \[hep-th\]](#).
- [26] J. Fuchs, I. Runkel, and C. Schweigert, TFT construction of RCFT correlators IV: Structure constants and correlation functions, *Nucl. Phys. B* **715**, 539 (2005), [arXiv:hep-th/0412290](#).
- [27] Z.-C. Gu, M. Levin, B. Swingle, and X.-G. Wen, Tensor-product representations for string-net condensed states, *Phys. Rev. B* **79**, 085118 (2009).
- [28] O. Buerschaper, M. Aguado, and G. Vidal, Explicit tensor network representation for the ground states of string-net models, *Phys. Rev. B* **79**, 085119 (2009).
- [29] D. Gaiotto and J. Kulp, Orbifold groupoids, *JHEP* **02**, 132, [arXiv:2008.05960 \[hep-th\]](#).
- [30] Y.-H. Lin, M. Okada, S. Seifnashri, and Y. Tachikawa, Asymptotic density of states in 2d CFTs with non-invertible symmetries, *JHEP* **03**, 094, [arXiv:2208.05495 \[hep-th\]](#).
- [31] G. Li, K. H. Pai, and Z.-C. Gu, Tensor-network renormalization approach to the  $q$ -state clock model, *Phys. Rev. Res.* **4**, 023159 (2022).
- [32] M. Bal, M. Mariën, J. Haegeman, and F. Verstraete, Renormalization group flows of hamiltonians using tensor networks, *Phys. Rev. Lett.* **118**, 250602 (2017).

### Convention for 6j-symbols and F symbols

The crossing kernels  $[F_l^{ijk}]_{mn}$  after being rescaled in the main text, which are often also referred to as the Racah coefficients in the literature, are related to quantum 6j-symbols as follows:

$$F_{mn} \begin{bmatrix} j & k \\ i & l \end{bmatrix} = \sqrt{d_m d_n} \begin{bmatrix} i & j & m \\ k & l & n \end{bmatrix}. \quad (38)$$

The quantum 6j symbols denoted by object in square brackets, enjoy full tetrahedral symmetry. In this gauge it fixes a number of components to:

$$\begin{bmatrix} a & a & 0 \\ b & b & c \end{bmatrix} = \begin{bmatrix} a & b & c \\ b & a & 0 \end{bmatrix} = \frac{N_{ab}^c}{\sqrt{d_a d_b}}. \quad (39)$$

Correspondingly,

$$[F_b^{aab}]_{0c} = \sqrt{\frac{d_c}{d_a d_b}}. \quad (40)$$

As described in the main text, the Racah coefficients are related to the crossing kernels describing crossing relations between canonically normalised conformal blocks by a re-scaling.

For the Ising CFT, the  $F^{\text{blocks}}$  are given by the expressions below with the parameter  $\lambda = 1/2$ :

$$F_{11} \begin{bmatrix} \psi & \psi \\ \psi & \psi \end{bmatrix} = 1, \quad (41)$$

$$F_{11} \begin{bmatrix} \sigma & \sigma \\ \sigma & \sigma \end{bmatrix} = -F_{\psi\psi} \begin{bmatrix} \sigma & \sigma \\ \sigma & \sigma \end{bmatrix} = \frac{1}{\sqrt{2}}, \quad (42)$$

$$F_{1\psi} \begin{bmatrix} \sigma & \sigma \\ \sigma & \sigma \end{bmatrix} = \frac{\lambda}{\sqrt{2}}, \quad F_{\psi 1} \begin{bmatrix} \sigma & \sigma \\ \sigma & \sigma \end{bmatrix} = \frac{1}{\sqrt{2}\lambda}, \quad (43)$$

$$F_{1\sigma} \begin{bmatrix} \psi & \sigma \\ \psi & \sigma \end{bmatrix} = F_{1\sigma} \begin{bmatrix} \sigma & \psi \\ \sigma & \psi \end{bmatrix} = \lambda, \quad (44)$$

$$F_{\sigma 1} \begin{bmatrix} \psi & \psi \\ \sigma & \sigma \end{bmatrix} = F_{\sigma 1} \begin{bmatrix} \sigma & \sigma \\ \psi & \psi \end{bmatrix} = \frac{1}{\lambda}, \quad (45)$$

$$F_{\sigma\sigma} \begin{bmatrix} \psi & \sigma \\ \sigma & \psi \end{bmatrix} = F_{\sigma\sigma} \begin{bmatrix} \sigma & \psi \\ \psi & \sigma \end{bmatrix} = -1. \quad (46)$$

The Racah coefficients of the Ising model are given by the same expressions above with  $\lambda = 1$ . The corresponding 6j symbols are given by

$$\begin{aligned} \begin{bmatrix} \sigma & \sigma & 1 \\ \sigma & \sigma & 1 \end{bmatrix} &= \begin{bmatrix} \sigma & \sigma & 1 \\ \sigma & \sigma & \psi \end{bmatrix} = \frac{1}{\sqrt{2}}, \quad \begin{bmatrix} \sigma & \sigma & \psi \\ \sigma & \sigma & \psi \end{bmatrix} = \frac{-1}{\sqrt{2}}, \quad (47) \\ \begin{bmatrix} 1 & 1 & 1 \\ \sigma & \sigma & \sigma \end{bmatrix} &= \begin{bmatrix} 1 & \psi & \psi \\ \sigma & \sigma & \sigma \end{bmatrix} = 2^{-\frac{1}{4}}. \quad (48) \end{aligned}$$

One can readily check that they are indeed related to  $F^{\text{blocks}}$  by a rescaling of the form

$$[F_l^{ijk}]_{mn} = [F_l^{ijk}]_{mn}^{\text{blocks}} \frac{\mathcal{N}_{jkn} \mathcal{N}_{inl}}{\mathcal{N}_{ijm} \mathcal{N}_{mkl}}. \quad (49)$$

### Another choice of conformal map – pants-diagram

In this section we give another conformal map that helps to calculate tensor as three point functions on the UHP. In this approach we prepare the states from asymptotic infinity and evolve them in Euclidean time to the triangle boundary. Thereby we extend the triangular region as a pants-diagram, as shown in Fig. 14. The function  $\chi$  is constructed by a map from pants-diagram to UHP.

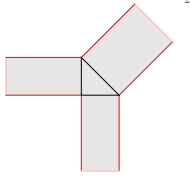


FIG. 14: pants-diagram

First we adopt the Schwarz–Christoffel transformation to find the map from upper-half-plane to the pants-diagram,

$$s(\xi) = \int^\xi dx \frac{\sqrt{2}(5x^2 - 1)^{\frac{1}{4}}}{x(x^2 - 1)}. \quad (50)$$

This function maps the three points  $-1, 0$  and  $1$  of the UHP to three infinities along the legs of pants, where we attach free open string states. Near these infinities, we have the following expansions:

$$\begin{aligned} s|_{\xi \rightarrow 1} &\sim \ln |\xi - 1|, \quad s|_{\xi \rightarrow 0} \sim -(1+i) \ln |\xi| + i\pi, \\ s|_{\xi \rightarrow -1} &\sim i \ln |\xi + 1| + \pi. \end{aligned} \quad (51)$$

These are precisely the functions we can utilize to prepare open string states at infinities. According to these relations, we define the conformal functions,

$$\begin{aligned} \chi_1(z) &:= s^{-1}(\ln z), \quad \chi_2(z) := s^{-1}(i \ln z + \pi), \\ \chi_3(z) &:= s^{-1}(-(1+i) \ln z + i\pi). \end{aligned} \quad (52)$$

It's hard to find a concise expression for the inverse function of the map  $s(\xi)$ . Instead, we expand this function around the singularities. This gives us the series expansion for  $\chi_i$ 's around  $z = 0$  as,

$$\begin{aligned} \chi_1(z) &= 1 + 0.9z + 0.709z^2 + 0.641z^3 + O(z^4) \\ \chi_2(z) &= -1 + 0.9z - 0.709z^2 + 0.641z^3 + O(z^4) \\ \chi_3(z) &= 0.410z + 0.008z^3 + O(z^5) \end{aligned} \quad (53)$$

This allows us to evaluate the tensor numerically. Again, we present the tensor component for primary fields following the steps in (19)

$$\alpha_{000}^{\Delta_1 \Delta_2 \Delta_3} \approx 0.671^{\Delta_1 + \Delta_2} 0.905^{\Delta_3}. \quad (54)$$

### More details on the transfer matrix

For our construction of FP tensor and the transfer matrix, the eigenvalue reproduce bulk state spectrum is expected because the trace of transfer matrix has a straight forward geometric meaning. The contraction of opposite legs of FP tensor corresponds to gluing the opposing edges of the square-shaped region, as depicted in Fig. 15. The outcome of this procedure is a path integral on a torus with a hole on the surface. As described in the main text, the weighted sum of boundary states residing on this small hole can be projected to the ground state as the size of the hole is reduced to zero.

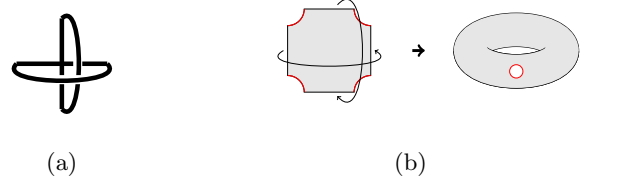


FIG. 15: Contraction the opposite legs of fixed point tensor produces partition function on torus.

To obtain the closed string spectrum, we tiling multiple tensors into a cylinder, as shown in Fig. 12. For the case where we use  $n$ -number of rank-4 tensors in the tiling process, the trace computes a torus partition function with moduli  $\tau = \frac{1}{n}$ ,

$$\text{Tr}(M_n) = \sum_i e^{\frac{2\pi}{n}(\frac{c}{12} - \Delta_i)}. \quad (55)$$

In order for this equation to be true for arbitrary value of  $n$ , the transfer matrix  $M_n$  must be able to diagonalize and give rise the following spectrum of CFT bulk states.

$$\lambda_n(i) = e^{\frac{2\pi}{n}(\frac{c}{12} - \Delta_i)} \quad (56)$$

State/Cutoff	007	117	227	337	447	exact
$\mathbb{1}$	0.0000	0.0000	0.0000	0.0000	0.0000	0.0000
$\sigma$	0.1245	0.1249	0.1249	0.1250	0.1250	0.1250
$\epsilon$	1.0293	1.0029	0.9930	0.9963	0.9989	1.0000
$\partial\sigma, \bar{\partial}\sigma$	1.1708	1.1324	1.1255	1.1237	1.1253	1.1250
$\partial\epsilon, \bar{\partial}\epsilon$	2.1345	2.0196	2.0030	1.9985	2.0004	2.0000
$\mathbb{1}^{(-2)}, \bar{\mathbb{1}}^{(-2)}$	2.2234	2.0301	1.9859	1.9899	1.9986	2.0000
$\partial\bar{\partial}\sigma$	2.3037	2.1449	2.1227	2.1045	2.1099	2.1250
$\sigma^{(-2)}, \bar{\sigma}^{(-2)}$	2.5273	2.1591	2.1330	2.1086	2.1208	2.1250
$\partial\bar{\partial}\epsilon$	3.0715	3.0345	2.9904	2.9384	2.9517	3.0000
$\partial^2\epsilon, \bar{\partial}^2\epsilon$	2.9115	3.0568	2.9732	2.9929	3.0030	3.0000
$\mathbb{1}^{(-3)}, \bar{\mathbb{1}}^{(-3)}$	2.9839	3.0491	2.9849	2.9333	2.9496	3.0000
$\bar{\partial}\sigma^{(-2)}, \partial\bar{\sigma}^{(-2)}$	3.0689	3.1085	3.0083	2.9444	2.9900	3.1250
$\partial\sigma^{(-2)}, \bar{\partial}\bar{\sigma}^{(-2)}$	3.6670	3.1805	3.0902	3.1065	3.1167	3.1250
$\sigma^{(-3)}, \bar{\sigma}^{(-3)}$	3.6973	3.2351	3.1346	3.1085	3.1291	3.1250
$\mathbb{1}^{(-2,-2)}$	4.0464	4.0442	4.0446	4.0431	4.0323	4.0000

TABLE VIII: Data from cylinder with length  $n = 4$ . Columns are labeled by the cutoff in descendant levels of the three legs of tensor. The actual bond dimensions correspond to the number of fields up to the specified descendant level cutoff. For instance, the bond dimensions for a cutoff of 447 is (7,7,22).

In the calculation of the FP tensor, a normalization prefactor always appears. However, this can be eliminated by considering the following ratio.

$$\frac{\lambda_2(0)}{\lambda_1(0)^2} = e^{-\frac{\pi}{4}c}. \quad (57)$$

This way we obtain the central charge  $c$ . The value computed from the transfer matrix is listed in the Table IV and Table VII.

In the following, we provide the spectrum data calculated from various cylinder moduli and bond dimensions in Table VIII, IX, X. Each column in these tables is labeled according to the cutoff in descendant levels for the fields on the three tensor legs. For example, 447 means that the short edges of the triangle have descendent level cut-off 4 while the long edge has descendant level cut-off 7. The data clearly demonstrate a consistent convergence of the computed conformal dimension towards the precise value as the cutoff increases.

### Gauge transformation

To compare our construction of FP tensor with that obtained from TNR method, we have to pick a particular gauge. One convenient choice of the gauge is to rotate the tensor leg to the basis which diagonalizes the transfer matrix  $M_{aiI,bjJ}$ ,

$$\sum_{a,b,i,I,j,J} M_{aiI,bjJ} O_{aiI}^r O_{bjJ}^s = e^{-2\pi\Delta_r} \delta_{rs} \quad (58)$$

State/Cutoff	007	117	227	337	447	exact
$\mathbb{1}$	0.0000	0.0000	0.0000	0.0000	0.0000	0.0000
$\sigma$	0.1241	0.1248	0.1249	0.1250	0.1250	0.1250
$\epsilon$	1.0541	1.0051	0.9878	0.9935	0.9980	1.0000
$\partial\sigma, \bar{\partial}\sigma$	1.2115	1.1380	1.1258	1.1226	1.1253	1.1250
$\partial\epsilon, \bar{\partial}\epsilon$	2.1398	2.0356	1.9798	1.9873	1.9924	2.0000
$\mathbb{1}^{(-2)}, \bar{\mathbb{1}}^{(-2)}$	2.2034	2.0554	2.0090	1.9902	2.0038	2.0000
$\partial\bar{\partial}\sigma$	2.2050	2.1618	2.0870	2.1022	2.1204	2.1250
$\sigma^{(-2)}$	2.3574	2.1582	2.0954	2.0576	2.0737	2.1250

TABLE IX: Data from cylinder with length  $n = 3$ .

State/Cutoff	007	117	227	337	447	exact
$\mathbb{1}$	0.0000	0.0000	0.0000	0.0000	0.0000	0.0000
$\sigma$	0.1231	0.1247	0.1246	0.1250	0.1250	0.1250
$\epsilon$	1.1146	0.9751	1.0110	0.9862	0.9955	1.0000
$\partial\sigma, \bar{\partial}\sigma$	1.3039	1.1313	1.1401	1.1166	1.1232	1.1250

TABLE X: Data from cylinder with length  $n = 2$ .

Using the same orthogonal matrix  $O$  we can rotate the rank-3 tensor to the same basis,

$$\tilde{\mathcal{T}}_{rst} = \sum_{a,i,I,j,J,k,K} \mathcal{T}_{(i,I)(j,J)(k,K)}^{aaa} O_{aiI}^r O_{ajJ}^s O_{ckK}^t. \quad (59)$$

In Ising CFT, we calculate the rank-3 tensor in diagonal basis and list the leading components in Table XI.

These tensor values can be fit by the three point function of bulk operators. We have normalized the first component to  $T_{000} = 1$ .

$$\tilde{\mathcal{T}}_{rst} \approx C_{rst} L^{\Delta_r - \Delta_s - \Delta_t} L^{\Delta_s - \Delta_r - \Delta_t} (\sqrt{2}L)^{h_t - h_r - h_s} \quad (60)$$

with  $L \approx 2.2$ , this matches with the result from numerical TNR [31][12].

### Entanglement filtering

In the numerical TNR method, besides the SVD decomposition and coarse-graining step there is an additional procedure called entanglement filtering. Intuitively the purpose of this step is to remove the short

Components	$\tilde{\mathcal{T}}_{rst}$
000	1.000
101	0.801
110	0.727
202	0.203
220	0.105
121	0.091
112	0.187

TABLE XI: The rank-3 FP tensor in diagonal basis.

range entanglement hidden in the tensor network and thereby get rid of the unphysical components of the tensor.

There are several ways to achieve this goal. One of them is plotted in Fig. 16. This procedure is performed for loops in the tensor network [5][10]. Entanglement filtering corresponds to minimizing the dimension of internal legs within the loop.



FIG. 16: Entanglement filtering procedure. The bond dimension cut-off of internal loop legs being optimized from  $D$  to  $D' < D$ .

Here we comment that the FP tensor we constructed in this work minimizes the bond dimension cut-off, at least asymptotically. This is because the d.o.f.'s in each leg of FP tensor corresponds to primary and descendant fields of CFT. They are ordered according to their conformal

dimensions  $h_i$ . Since their contribution to the tensor value is proportional to  $e^{-h_i}$ , the induced error by a conformal dimension cut-off  $h_{cut}$  is proportional to  $e^{-h_{cut}}$ . A general change of basis in the internal legs changes the ordering of these states and therefore likely to increase the error by keeping the same number of states.

Another method in TNR for entanglement filtering is to maintain the positivity of local Hamiltonian in each step of RG [32]. Our FP tensor also satisfies this property, since each rank-4 tensor is computed from the Euclidean path-integral in a square-shaped patch, see Fig. 17. It can be naturally viewed as an Euclidean time evolution from the *in*-states to the *out*-states with the CFT Hamiltonian which is positive for unitary models.

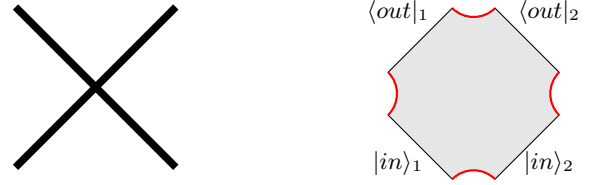


FIG. 17: The rank-4 tensor can be viewed as a Euclidean time evolution using the CFT Hamiltonian.

### Structure constant for tri-critical Ising CFT

$C_{\Phi\Phi\Phi}^{\Phi\Phi\Phi}$	0.7862	$C_{\Phi\Phi\Phi}^{\Phi\Phi\Phi}$	0.7862	$C_{\Phi\Phi\Phi}^{\Phi\Phi\Phi}$	-0.4281	$C_{\Phi\Phi\Phi}^{\Psi\Phi\Phi}$	0.7862	$C_{\Phi\Phi\Phi}^{\Psi\Phi\Phi}$	0.7862	$C_{\Phi\Phi\Phi}^{\Phi\Phi\Psi}$	0.4281	$C_{\Phi\Phi\Phi}^{\Psi\Phi\Psi}$	-0.6927	$C_{\Phi\Phi\Phi}^{\Phi\Phi\Psi}$	0.6927	$C_{\Phi\Phi\Phi}^{\Psi\Phi\Psi}$	0.5147	$C_{\Phi\Phi\Phi}^{\Psi\Phi\Psi}$	0.7862
$C_{\Psi\Phi\Phi}^{\Psi\Phi\Phi}$	0.7862	$C_{\Psi\Phi\Phi}^{\Psi\Phi\Phi}$	-0.4281	$C_{\Phi\Phi\Phi}^{\Omega\Lambda\Omega}$	0.6611	$C_{\Phi\Phi\Phi}^{\Omega\Lambda\Omega}$	0.6611	$C_{\Phi\Phi\Phi}^{\Omega\Lambda\Omega}$	-0.5825	$C_{\Phi\Phi\Phi}^{\Omega\Lambda\Omega}$	0.36	$C_{\Phi\Phi\Phi}^{\Omega\Lambda\Omega}$	0.5825	$C_{\Phi\Phi\Phi}^{\Omega\Lambda\Omega}$	0.4328	$C_{\Phi\Phi\Phi}^{\Omega\Lambda\Omega}$	-0.4328	$C_{\Phi\Phi\Phi}^{\Omega\Lambda\Omega}$	0.6611
$C_{\Psi\Phi\Phi}^{\Omega\Lambda\Omega}$	0.6611	$C_{\Psi\Phi\Phi}^{\Omega\Lambda\Omega}$	-0.36	$C_{\Psi\Phi\Phi}^{\Omega\Lambda\Omega}$	0.5825	$C_{\Psi\Phi\Phi}^{\Omega\Lambda\Omega}$	-0.4674	$C_{\Psi\Phi\Phi}^{\Omega\Lambda\Omega}$	0.4674	$C_{\Psi\Phi\Phi}^{\Omega\Lambda\Omega}$	0.4409	$C_{\Psi\Phi\Phi}^{\Omega\Lambda\Omega}$	0.4674	$C_{\Psi\Phi\Phi}^{\Omega\Lambda\Omega}$	0.4674	$C_{\Psi\Phi\Phi}^{\Omega\Lambda\Omega}$	-0.4409	$C_{\Psi\Phi\Phi}^{\Omega\Lambda\Omega}$	-0.18
$C_{\Psi\Phi\Phi}^{\Omega\Lambda\Psi}$	-0.2912	$C_{\Psi\Phi\Phi}^{\Omega\Lambda\Psi}$	0.5725	$C_{\Psi\Phi\Phi}^{\Lambda\Lambda\Lambda}$	0.8409	$C_{\Psi\Phi\Phi}^{\Lambda\Lambda\Lambda}$	0.8409	$C_{\Psi\Phi\Phi}^{\Lambda\Lambda\Lambda}$	-0.8409	$C_{\Psi\Phi\Phi}^{\Lambda\Lambda\Lambda}$	0.6611	$C_{\Psi\Phi\Phi}^{\Lambda\Lambda\Lambda}$	0.6611	$C_{\Psi\Phi\Phi}^{\Lambda\Lambda\Lambda}$	-0.6611	$C_{\Psi\Phi\Phi}^{\Lambda\Lambda\Lambda}$	0.6611	$C_{\Psi\Phi\Phi}^{\Lambda\Lambda\Lambda}$	0.6611
$C_{\Omega\Lambda\Omega}^{\Omega\Lambda\Omega}$	0.6611	$C_{\Omega\Lambda\Omega}^{\Omega\Lambda\Omega}$	0.6611	$C_{\Omega\Lambda\Omega}^{\Omega\Lambda\Omega}$	0.6611	$C_{\Omega\Lambda\Omega}^{\Omega\Lambda\Omega}$	0.2912	$C_{\Omega\Lambda\Omega}^{\Omega\Lambda\Omega}$	-0.7134	$C_{\Omega\Lambda\Omega}^{\Omega\Lambda\Omega}$	-0.0883	$C_{\Omega\Lambda\Omega}^{\Omega\Lambda\Omega}$	1.0	$C_{\Omega\Lambda\Omega}^{\Omega\Lambda\Omega}$	0.7862	$C_{\Omega\Lambda\Omega}^{\Omega\Lambda\Omega}$	0.7862	$C_{\Omega\Lambda\Omega}^{\Omega\Lambda\Omega}$	1.0
$C_{\Omega\Lambda\Omega}^{\Psi\Phi\Phi}$	1.0	$C_{\Omega\Lambda\Omega}^{\Psi\Phi\Phi}$	1.0	$C_{\Omega\Lambda\Omega}^{\Psi\Phi\Phi}$	1.0	$C_{\Omega\Lambda\Omega}^{\Lambda\Lambda\Lambda}$	0.8409	$C_{\Omega\Lambda\Omega}^{\Omega\Lambda\Omega}$	0.6611	$C_{\Omega\Lambda\Omega}^{\Lambda\Lambda\Lambda}$	0.8409	$C_{\Omega\Lambda\Omega}^{\Lambda\Lambda\Lambda}$	0.8409	$C_{\Omega\Lambda\Omega}^{\Lambda\Lambda\Lambda}$	0.8409	$C_{\Omega\Lambda\Omega}^{\Lambda\Lambda\Lambda}$	0.6611	$C_{\Omega\Lambda\Omega}^{\Lambda\Lambda\Lambda}$	0.5505

TABLE XII: Structure Constant

### Iteration relations

*Transformation rules* — In this section, we present details in mapping descendant fields under a conformal transformation  $\chi(z)$ . For more general descendant fields, we can not give a simple expression for the transformation coefficients, but deriving an iteration relation is possible.

Suppose that we already know the transformation rule for the operator  $O^{(-k_l, \dots, -k_2, -k_1)} := L_{-k_l} \dots L_{-k_2} L_{-k_1} O$ . The transformation under holomorphic function  $\chi(z)$  is written as

$$\chi_* O^{(-k_l, \dots, -k_2, -k_1)}(z) = \sum_{\{k'\} \leq \{k\}} H_{k'_l, \dots, k'_2, k'_1}^{k_l, \dots, k_2, k_1}(z) O^{(-k'_l, \dots, -k'_2, -k'_1)}(\eta). \quad (61)$$

where  $\eta = \chi(z)$ , and the symbol  $\{k\}$  is a shorthand notation of  $\{k_l, \dots, k_2, k_1\}$ .  $\{k'\} \leq \{k\}$  means that  $\forall k_i \in \{k\}$ ,

$k'_i \leq k_i$ . Moreover, suppose that we also know the OPE between  $T(z)$  and  $O^{(-k_l, \dots, -k_2, -k_1)}(z')$ :

$$\begin{aligned} T(z)O^{(-k_l, \dots, -k_2, -k_1)}(z') &= \sum_{k'_{l+1}} (z - z')^{k'_{l+1}-2} O^{(-k'_{l+1}, -k_l, \dots, -k_2, -k_1)}(z') \\ &+ \sum_{\{k'\} \leq \{k\}} \frac{C_{k'_l, \dots, k'_2, k'_1}^{k_l, \dots, k_2, k_1}}{(z - z')^{\sum_{p=1}^l k_p - \sum_{p=1}^l k'_p + 2}} O^{(-k'_l, \dots, -k'_2, -k'_1)}(z'). \end{aligned} \quad (62)$$

Then we can derive the transformation rule for higher level descendant field  $O^{(-k_{l+1}, -k_l, \dots, -k_2, -k_1)}$  as

$$\begin{aligned} &\chi_* O^{(-k_{l+1}, -k_l, \dots, -k_2, -k_1)}(z') \\ &= \oint_{z'} \frac{dz}{2\pi i} (z - z')^{1-k_{l+1}} \chi_* T(z) \chi_* O^{(-k_l, \dots, -k_2, -k_1)}(z') \\ &= \oint_{\eta'} \frac{d\eta}{2\pi i} \frac{(z - z')^{1-k_{l+1}}}{\chi'(z)} [\chi'(z)^2 T(\eta) + \frac{c}{12} \{\chi(z), z\}] \sum_{\{k'\} \leq \{k\}} H_{k'_l, \dots, k'_2, k'_1}^{k_l, \dots, k_2, k_1}(z') O^{(-k'_l, \dots, -k'_2, -k'_1)}(\eta') \\ &= \sum_{\{k'\} \leq \{k\}} \sum_{k'_{l+1}=0}^{k_{l+1}} H_{k'_l, \dots, k'_2, k'_1}^{k_l, \dots, k_2, k_1}(z') a_{k_{l+1}-k'_{l+1}}^{k_{l+1}}(z') O^{(-k'_{l+1}, -k'_l, \dots, -k'_2, -k'_1)}(\eta') \\ &+ \sum_{\{k''\} \leq \{k\}} \left[ \sum_{\{k'\} \leq \{k''\} \leq \{k\}} H_{k'_l, \dots, k'_2, k'_1}^{k_l, \dots, k_2, k_1}(z') a_{k_{l+1}+\sum k'' - \sum k'}^{k_{l+1}}(z') C_{k'_l, \dots, k'_2, k'_1}^{k'_l, \dots, k'_2, k'_1} \right] O^{(-k'_l, \dots, -k'_2, -k'_1)}(\eta') \\ &+ \frac{c}{12(k_{l+1}-2)!} \left( \frac{d}{dz} \right)^{k_{l+1}-2} \{\chi(z), z\} \Big|_{z=z'} \sum_{\{k'\} \leq \{k\}} H_{k'_l, \dots, k'_2, k'_1}^{k_l, \dots, k_2, k_1}(z') O^{(-k'_l, \dots, -k'_2, -k'_1)}(\eta'), \end{aligned} \quad (63)$$

where the coefficients  $a_m^n$ 's are defined by

$$\chi'(z)(z - z')^{1-n} = (\eta - \eta')^{1-n} \sum_{m=0}^{\infty} a_m^n(z') (\eta - \eta')^m. \quad (64)$$

Comparing with the definition of these transformation coefficients we conclude that,

$$\begin{aligned} H_{k'_{l+1}, k'_l, \dots, k'_2, k'_1}^{k_{l+1}, k_l, \dots, k_2, k_1}(z') &= H_{k'_l, \dots, k'_2, k'_1}^{k_l, \dots, k_2, k_1}(z') a_{k_{l+1}-k'_{l+1}}^{k_{l+1}}(z') \\ H_{k'_{l+1}, k_l, \dots, k_2, k_1}^{k_{l+1}, k_l, \dots, k_2, k_1}(z') &= \sum_{\{k'\} \leq \{k''\} \leq \{k\}} a_{k_{l+1}+\sum k'' - \sum k'}^{k_{l+1}}(z') H_{k'_l, \dots, k'_2, k'_1}^{k_l, \dots, k_2, k_1}(z') C_{k'_l, \dots, k'_2, k'_1}^{k'_l, \dots, k'_2, k'_1} \\ &+ \frac{c}{12(k_{l+1}-2)!} \left( \frac{d}{dz} \right)^{k_{l+1}-2} \{\chi(z), z\} \Big|_{z=z'} H_{k'_l, \dots, k'_2, k'_1}^{k_l, \dots, k_2, k_1}(z'). \end{aligned} \quad (65)$$

*OPE coefficients* — Now we derive an iteration relation of the OPE coefficient between energy momentum tensor  $T(z)$  and a general descendant field  $O^{(-k_l, \dots, -k_2, -k_1)}(z')$ . The OPE coefficients are denoted by the symbol  $C_{k'_l, \dots, k'_2, k'_1}^{k_l, \dots, k_2, k_1}$  defined as,

$$\begin{aligned} T(z)O^{(-k_l, \dots, -k_2, -k_1)}(z') &= \sum_{k'_{l+1}=1}^{\infty} (z - z')^{k'_{l+1}-2} O^{(-k'_{l+1}, -k_l, \dots, -k_2, -k_1)}(z') \\ &+ \sum_{\{k'\} \leq \{k\}} \frac{C_{k'_l, \dots, k'_2, k'_1}^{k_l, \dots, k_2, k_1}}{(z - z')^{\sum_{p=1}^l k_p - \sum_{p=1}^l k'_p + 2}} O^{(-k'_l, \dots, -k'_2, -k'_1)}(z'). \end{aligned} \quad (66)$$

Again, we use the symbol  $\{k\}$  to denote the set  $\{k_l, \dots, k_2, k_1\}$ .  $\{k'\} \leq \{k\}$  means that  $k'_p \leq k_p$  for any  $1 \leq p \leq l$ .

For the higher level descendants  $O^{(-k_{l+1}, -k_l, \dots, -k_2, -k_1)}$ , its operator product with  $T(z)$  is,

$$\begin{aligned}
& T(z)O^{(-k_{l+1}, -k_l, \dots, -k_2, -k_1)}(z') \\
&= \oint_{z'} \frac{dw}{2\pi i} (w - z')^{1-k_{l+1}} T(z) T(w) O^{(-k_l, \dots, -k_2, -k_1)}(z') \\
&= - \left[ \oint_z \frac{dw}{2\pi i} (w - z')^{1-k_{l+1}} T(w) T(z) \right] O^{(-k_l, \dots, -k_2, -k_1)}(z') + \oint_{z'} \frac{dw}{2\pi i} (w - z')^{1-k_{l+1}} T(w) [T(z) O^{(-k_l, \dots, -k_2, -k_1)}(z')] \\
&= \sum_{k'_{l+1}=1}^{k_{l+1}} (2k_{l+1} - k'_{l+1}) \frac{O^{(-k'_{l+1}, -k_l, \dots, -k_2, -k_1)}}{(z - z')^{k_{l+1} - k'_{l+1} + 2}} + \sum_{\{k'\} \leq \{k\}} C_{k'_l, \dots, k'_2, k'_1}^{k_l, \dots, k_2, k_1} \frac{O^{(-k_{l+1}, -k'_l, \dots, -k'_2, -k'_1)}(z')}{(z - z')^{\sum_{p=1}^l k_p - \sum_{p=1}^l k'_p + 2}} \\
&\quad + \sum_{\{k'\} \leq \{k\}} (2k_{l+1} + \sum_{p=1}^l k_p - \sum_{p=1}^l k'_p) C_{k'_l, \dots, k'_2, k'_1}^{k_l, \dots, k_2, k_1} \frac{O^{(-k'_l, \dots, -k'_2, -k'_1)}(z')}{(z - z')^{k_{l+1} + \sum_{p=1}^l k_p - \sum_{p=1}^l k'_p + 2}} \\
&\quad + \frac{c}{12} k_{l+1} (k_{l+1}^2 - 1) \frac{O^{(-k_l, \dots, -k_2, -k_1)}}{(z - z')^{k_{l+1} + 2}} + \dots
\end{aligned} \tag{67}$$

where the ellipsis denotes any combination of descendant operators at level higher than  $\sum_{p=1}^{l+1} k_p$ . We neglected them simply because we already know their coefficients.

Comparing with the definition of  $C_{k'_{l+1}, k'_l, \dots, k'_2, k'_1}^{k_{l+1}, k_l, \dots, k_2, k_1}$ , we conclude that,

$$\begin{aligned}
C_{k'_{l+1}, k_l, \dots, k_2, k_1}^{k_{l+1}, k_l, \dots, k_2, k_1} &= 2k_{l+1} - k'_{l+1}, \quad \text{for } 1 \leq k'_{l+1} < k_{l+1} \\
C_{k_{l+1}, k'_l, \dots, k'_2, k'_1}^{k_{l+1}, k_l, \dots, k_2, k_1} &= C_{k'_l, \dots, k'_2, k'_1}^{k_l, \dots, k_2, k_1}, \quad \text{for } \{k'\} < \{k\} \\
C_{k_{l+1}, k_l, \dots, k_2, k_1}^{k_{l+1}, k_l, \dots, k_2, k_1} &= k_{l+1} + C_{k_l, \dots, k_2, k_1}^{k_l, \dots, k_2, k_1} \\
C_{k'_l, \dots, k'_2, k'_1}^{k_{l+1}, k_l, \dots, k_2, k_1} &= (2k_{l+1} + \sum_{p=1}^l k_p - \sum_{p=1}^l k'_p) C_{k'_l, \dots, k'_2, k'_1}^{k_l, \dots, k_2, k_1} + \frac{c}{12} k_{l+1} (k_{l+1}^2 - 1) \delta_{\{k'\}}^{\{k\}}
\end{aligned} \tag{68}$$

*Correlation function* — We can also derive an iteration equation of correlators. Suppose that we already know all the correlators of lower level descendants, we can derive the higher level ones using this equation.

To simplify the notation, we use  $O^{(-\vec{k})}$  to denote  $O^{(-k_l, \dots, -k_2, -k_1)}$ , and the OPE coefficient  $C_{\vec{k}'}^{\vec{k}}$  to denote  $C_{k'_l, \dots, k'_2, k'_1}^{k_l, \dots, k_2, k_1}$ .

Then we will show that the correlator  $\langle L_{-m} O_1^{(-\vec{k})}(x) O_2^{(-\vec{p})}(y) O_3^{(-\vec{q})}(z) \rangle$  can be written as a linear combination of simpler correlators of the form  $\langle O_1^{(-\vec{k}')} (x) O_2^{(-\vec{p}')} (y) O_3^{(-\vec{q}')} (z) \rangle$ , with  $\vec{k}' \leq \vec{k}$ ,  $\vec{p}' \leq \vec{p}$  and  $\vec{q}' \leq \vec{q}$  (in the sense of  $\{k'\} \leq \{k\}$  defined in the previous sections). We start from the equation,

$$\begin{aligned}
& \langle L_{-m} O_1^{(-\vec{k})}(x) O_2^{(-\vec{p})}(y) O_3^{(-\vec{q})}(z) \rangle \\
&= \oint_x \frac{dw}{2\pi i} (w - x)^{1-m} \langle [T(w) O_1^{(-\vec{k})}(x)] O_2^{(-\vec{p})}(y) O_3^{(-\vec{q})}(z) \rangle \\
&= - \oint_y \frac{dw}{2\pi i} (w - x)^{1-m} \langle O_1^{(-\vec{k})}(x) [T(w) O_2^{(-\vec{p})}(y)] O_3^{(-\vec{q})}(z) \rangle - \oint_z \frac{dw}{2\pi i} (w - x)^{1-m} \langle O_1^{(-\vec{k})}(x) O_2^{(-\vec{p})}(y) [T(w) O_3^{(-\vec{q})}(z)] \rangle
\end{aligned} \tag{69}$$

Using the OPE,

$$T(w) O^{(-\vec{p})}(y) = \sum_{\vec{p}' \leq \vec{p}} C_{\vec{p}'}^{\vec{p}} \frac{O^{(-\vec{p}')} (y)}{(w - y)^{|\vec{p}| - |\vec{p}'| + 2}} + \frac{\partial O^{(-\vec{p})}(y)}{w - y} + \text{reg.}, \tag{70}$$

where *reg.* means the regular terms in the limit  $w \rightarrow y$ , we can expand the expression,

$$\begin{aligned}
& \oint_y \frac{dw}{2\pi i} (w-x)^{1-m} \langle O_1^{(-\vec{k})}(x) [T(w) O_2^{(-\vec{p})}(y)] O_3^{(-\vec{q})}(z) \rangle \\
&= \frac{\partial_y}{(y-x)^{m-1}} \langle O_1^{(-\vec{k})}(x) O_2^{(-\vec{p})}(y) O_3^{(-\vec{q})}(z) \rangle \\
&+ (-1)^{|\vec{p}|-|\vec{p}'|-1} \sum_{\vec{p}' \leq \vec{p}} \frac{C_{\vec{p}'}^{\vec{p}}}{(y-x)^{m+|\vec{p}|-|\vec{p}'|}} \frac{(|\vec{p}'|-|\vec{p}'|+m-1)!}{(|\vec{p}'|-|\vec{p}'|+1)!(m-2)!} \langle O_1^{(-\vec{k})}(x) O_2^{(-\vec{p}')} (y) O_3^{(-\vec{q})}(z) \rangle.
\end{aligned} \tag{71}$$

The other term is calculated similarly. So the correlator is reduced to combinations of simpler ones:

$$\begin{aligned}
& \langle L_{-m} O_1^{(-\vec{k})}(x) O_2^{(-\vec{p})}(y) O_3^{(-\vec{q})}(z) \rangle \\
&= - \frac{\partial_y}{(y-x)^{m-1}} \langle O_1^{(-\vec{k})}(x) O_2^{(-\vec{p})}(y) O_3^{(-\vec{q})}(z) \rangle \\
&+ (-1)^{|\vec{p}|-|\vec{p}'|} \sum_{\vec{p}' \leq \vec{p}} \frac{C_{\vec{p}'}^{\vec{p}}}{(y-x)^{m+|\vec{p}|-|\vec{p}'|}} \frac{(|\vec{p}'|-|\vec{p}'|+m-1)!}{(|\vec{p}'|-|\vec{p}'|+1)!(m-2)!} \langle O_1^{(-\vec{k})}(x) O_2^{(-\vec{p}')} (y) O_3^{(-\vec{q})}(z) \rangle \\
&+ (y \rightarrow z, \vec{p} \rightarrow \vec{q}).
\end{aligned} \tag{72}$$